Exp Fluids (2017) 58:26
DOI 10.1007/s00348-017-2303-4

RESEARCH ARTICLE

Effect of instantaneous stirring process on mixing between initially distant scalars in turbulent obstacle wakes

F. Shoaei[1] · J. P. Crimaldi[1]

Received: 16 September 2016 / Revised: 19 January 2017 / Accepted: 20 January 2017

Abstract A two-channel planar laser-induced fluorescence technique is used to study mixing and reactions between two initially distant scalars in the turbulent wake of a cylindrical obstacle. The scalars are released continuously and isokinetically upstream of the cylinder, with a lateral separation that initially impedes mixing between them. The effect of the turbulent wake on mixing and reaction enhancement is determined by measuring the segregation parameter for cases with and without the cylinder obstruction. Results indicate that scalar mixing and reaction rates (in the low-Damkohler limit) increase significantly in the presence of the cylinder wake. The study also shows that the dominant contribution of total reaction derives from the scalar covariance associated with instantaneous flow processes, and depends strongly on streamwise location within the wake. The results have broad implications for mixing processes in engineering and ecology.

1 Introduction

1.1 The role of structured stirring on initially distant scalars

The ability of structured flow fields to impart spatial correlations onto a pair of initially distant scalars has been demonstrated numerically (Crimaldi and Browning 2004; Crimaldi et al. 2006, 2008) and experimentally (Soltys and Crimaldi 2015). This scalar coalescence occurs even for passive scalars where the dynamics of each scalar field evolves independently of the other; the structure of the shared velocity field is responsible for the coalescence. If the initial separation distance between the two scalars is smaller than the largest coherent length scales of the local flow, the two scalar fields develop similar instantaneous spatial distributions. While it is easier to envision these processes in simple flows, recent numerical simulations (Pratt et al. 2015) have shown that in more complex 2D flows involving multiple interacting vortices, initially distant scalars coalesce in regions of intense mixing and attracting Lagrangian coherent structures.

In aquatic ecosystems, structured flows can facilitate stirring and diffusion to enhance reactions or population growth by bringing together species and nutrients (e.g., Richards and Brentnall 2006). Structured flows stir any introduced scalars into thin filament shells (Garrett 1983), enhancing local scalar gradients, increasing the interfacial area of the scalar through chaotic stretching and folding (Hinch 1999), leading finally to increased mixing by molecular diffusion.

Structured flow can also contribute directly to the colocation of conspecifics or species competing for a resource (e.g., Károlyi et al. 2000). The presence of benthic aquatic fauna can itself lead to structured flow in wakes downstream of the organisms. Flow structure is also modified by benthic topology such as sea-mounts, and can be dominated by a vortex wake that produces mixing (Richards 1990). As a specific example, these stirring mechanisms may enhance fertilization rates for reproduction by benthic marine invertebrates, which reproduce by broadcast spawning: plumes of egg and sperm are released, at separate locations, into

✉ J. P. Crimaldi
crimaldi@colorado.edu

F. Shoaei
farrokh.shoaei@colorado.edu

[1] Department of Civil and Environmental Engineering, University of Colorado, Boulder, CO 80309-0428, USA

Published online: 18 March 2017

the ambient water and must coalesce for fertilization to occur (Miller and Mundy 2003; Jackson 1986).

1.2 Mixing of multiple reactive scalars

Turbulence exhibits complex instantaneous behavior resulting from chaotic interaction of coherent flow structures (Cantwell 1981; Adrian 2007). In flows with multiple reactive scalars, the reaction term couples the advection–diffusion equations for the two scalars (Mao and Toor 1971):

$$\frac{\partial C_1}{\partial t} = -U_i \cdot \nabla C_1 + D_1 \nabla^2 C_1 - \Theta \tag{1}$$

$$\frac{\partial C_2}{\partial t} = -U_i \cdot \nabla C_2 + D_2 \nabla^2 C_1 - \Theta. \tag{2}$$

The present study will focus on systems with two initially distant scalars in a second-order reaction given by

$$\Theta = kC_1C_2, \tag{3}$$

where k is the reaction rate constant and C_1 and C_2 are the local concentrations of the reactants. The relative strength of the reaction rate in a stirred system is governed by the nondimensional Damkohler number, Da, formed as a ratio of the reaction kinetics time constant to the diffusive timescale. It is common to study the potential for mixing processes to influence reaction rates in the low-Da limit $Da \to 0$ (e.g., Crimaldi et al. 2006, 2008; Crimaldi and Kawakami 2013); in this limit, the reaction has negligible effect on the existing scalar fields, and conserved scalars are proxies for studying and predicting potential reaction dynamics of stirred scalars.

Using a standard Reynolds decomposition (Adrian et al. 2000), the local scalar concentrations can be decomposed into the sum of a mean component (denoted by <>) and a fluctuating component relative to the mean (denoted with a prime): $C_1 = \langle C_1 \rangle + c_1'$, and $C_2 = \langle C_2 \rangle + c_2'$. By substituting these decompositions into Eq. 3 and then averaging, the averaged value of the normalized reaction rate Θ/k is then (Crimaldi et al. 2006)

$$\langle C_1C_2 \rangle = \langle C_1 \rangle \langle C_2 \rangle + \left\langle c_1'c_2' \right\rangle, \tag{4}$$

where the first term on the RHS is simply the product of the average concentrations, and the second term is the correlation between the fluctuating concentrations. The term $\langle C_1C_2 \rangle$ in Eq. 4 can be interpreted generally as a mean local mixing parameter, and as a metric for reactions in the low-Da limit. It is not uncommon for simple reaction models to consider only the effect of the mean concentrations (first term in Eq. 4). The present work aims to understand the role of instantaneous processes (second term in Eq. 4) on enhancements to mixing and reactions between two initially distant scalars in turbulent flow.

1.3 Cylinder wake mixing

Over a broad range of scales, bluff-body and cylinder wakes are universal in natural and engineered systems. At small scales, cylinder wakes are used as microfluidic reactors to mix chemicals (Deshmukh and Vlachos 2005; Wang and Hu 2010). At large scales, enhanced mixing and reaction are observed in wakes behind oceanic islands (Heywood et al. 1990; Dong and McWilliams 2007; Dong et al. 2007) with ecological implications on phytoplankton dynamics (Sandulescu et al. 2008) and nutrient distributions (Hasegawa et al. 2004).

Mixing and reactions in a laminar cylinder wake have been studied in the general context of nonlinear dynamics (Jung et al. 1993; Ziemniak et al. 1994; Tel et al. 2000), and in the biological context of species competition and coexistence (Scheuring et al. 2000, 2003). Previous numerical studies also looked at mixing and reaction in wakes (Froncioni et al. 1997; Celik and Beskok 2009; Crimaldi and Kawakami 2013). At laboratory scales, particularly for turbulent flows, mixing and reactions behind cylinders have been studied experimentally (Kastrinakis and Nychas 1998; Breidenthal 1981; Mi et al. 2004).

In the case of broadcast spawning described earlier, egg and sperm are released into the flow at separate locations and must coalesce locally at a downstream location for fertilization to occur (Crimaldi and Zimmer 2014). The flow environment in spawning regions can be influenced by unsteady vortex shedding in wakes behind obstacles (Ferrier et al. 1996; Guichard and Bourget 1998). The obstacles can be the reproducing adults themselves (e.g., urchins, coral heads), or irregularities in local bed topography. Unsteady wakes (e.g., Karman vortex streets) behind flow obstacles serve as effective reactors for bimolecular reactions (Kastrinakis and Nychas 1998; Toroczkai et al. 1998; Károlyi et al. 1999), and could thus enhance fertilization rates. Using broadcast spawning as motivation, the current study investigates how the turbulent wakes behind a circular cylinder can promote coalescence between initially distant scalars to facilitate reactions.

2 Experiment setup

2.1 Flow facility

The experiments were conducted in a recirculating flume with a test section that is 9 m long and 1.25 m wide. Flow from the head section of the flume first passes through a honeycomb flow straightener, and then through a wire mesh turbulence generation grid with wire diameter 0.55 cm and square mesh spacing 3.18 cm to produce turbulence that is approximately isotropic and homogenous. The grid

covers the entire width and depth of the flume. At the end of the test section, weir plates are used to adjust the running flow depth to 50 cm. Flow is driven through the test section by a pair of computer-controlled centrifugal pumps. The walls and bed of the flume are glass, permitting non-intrusive optical measurement techniques to be used to measure velocity and scalar fields.

2.2 Two-channel planar laser-induced fluorescence

A novel two-color planar laser-induced fluorescence (2C-PLIF) system (Fig. 1) has been used to quantify the spatial and temporal dispersion and coalescence of two initially distant scalars released in the flume. The 2C-PLIF system used in the present study is identical to that used and described in Soltys and Crimaldi (2011), and the reader is referred to that work for additional details about the system design, calibration, and validation.

Two fluorescent dyes, Fluorescein sodium salt (CAS# 518-47-8) and Oxazine 725 (CAS# 24796-94-9), are illuminated by a thin (100 μm) bispectral laser sheet comprised of two wavelengths (488 and 647.1 nm) of light from argon-ion and krypton-ion lasers, respectively. Peak absorption and emission wavelengths for each of the two dyes are listed in Table. 1. The two dyes each fluoresce light at different wavelengths, with an intensity (under appropriate conditions) proportional to local concentration (Soltys and Crimaldi 2011; Crimaldi 2008).

Time series of 12-bit, 1393×1040 pixel images are recorded from each camera. Each camera is fitted with a narrow-band filter that passes only one of the two fluoresced wavelengths. For a typical experiment, approximately 5000 images at 0.5 Hz are recorded from each camera for each scalar. Data is streamed to an image acquisition system. Each channel of the 2-C PLIF system was calibrated by injection a laminar jet of full-strength source dye into the measurement region. An image processing algorithm also calibrates the images and corrects them for errors caused by background fluorescence,

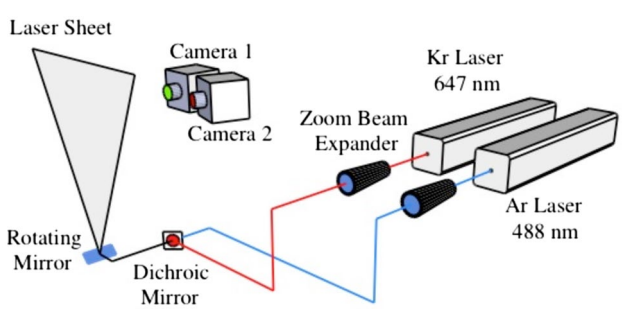

Fig. 1 Schematic of two-channel planar laser Induced fluorescence system as detailed in Soltys and Crimaldi (2011)

intensity variations in the laser scan, attenuation due to background dye, lens vignette, variations in camera pixel response, and camera dark response (Crimaldi 2008).

Since all of the fluorescence information within a single voxel (the volume imaged by a single pixel across the width of the laser sheet) is averaged to a single value, the spatial resolution of instantaneous PLIF images is determined by the area imaged by a single pixel and the sheet thickness. The scale of the smallest concentrations η_B in a flow is (Batchelor 1959)

$$\eta_B = \eta_K S_c^{-1/2} \tag{5}$$

where $S_c = \nu/D$ and η_K is the Kolmogorov scale. The molecular diffusivity D for the fluorescent dyes in water typically ranges from 1E−6 to 5E−6 cm^2/s (Crimaldi 2008), meaning that S_c ranges from 2000 to 9000. Thus, the smallest concentration scales in the flow are roughly 50–100 times smaller than the smallest scales of motion, and are often smaller than the spatial resolution of PLIF systems. However, the bulk of the scalar stirring and transport occurs at larger scales that are captured by the 2C-PLIF system. To compute a measure of the reaction rate, we use conservative scalars, and then compute the scalar overlap term C_1C_2 digitally after-the-fact; this scalar overlap term approaches the non-dimensional reaction in the low-Da limit.

2.3 Cylinder wake mixing experiment

The experimental setup to create a pair of initially distant plumes in a cylinder wake is shown schematically in Fig. 2. The scalars are introduced from a pair of copper tubes (2.75 m long with 0.56 cm diameter) to ensure a laminar flow with temperature that was equilibrated with the flume flow. Dye is pumped through these tubes using gear pumps to produce an isokinetic release. Dye concentrations were sufficiently low to be optically thin (Crimaldi 2008). PLIF data of undiluted source fluid were taken at the nozzle exits to determine the source concentration C_0 for each scalar; these concentrations are used to normalize all scalar results in the following section.

A cylindrical obstacle with diameter $\phi = 4.83$ cm can be placed in the test section to create a turbulent obstacle wake. Scalar mixing was investigated for two experimental configurations (with and without the cylinder), for two nozzle spacings ($s/\phi = 0.25$ and $s/\phi = 0.50$) and at two Reynolds numbers ($Re_\phi = 2000$ and $Re_\phi = 5000$). As shown in Fig. 2, scalar image data were acquired at two locations: an upstream location centered at $x/\phi = 8.75$, and at a downstream location centered at $x/\phi = 33$.

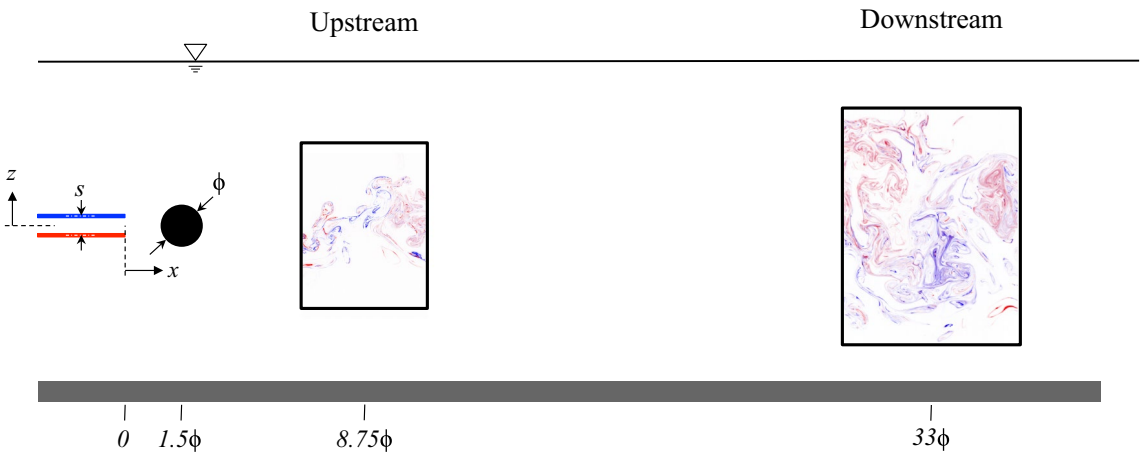

Fig. 2 Experimental configuration showing the location of the scalar release tubes (*red* and *blue lines*), cylinder (*black circle*), and upstream and downstream measurement locations (*black rectangles*). Also shown are the cylinder diameter, ϕ, nozzle spacing, s, and streamwise and transverse coordinates, x and z. The upstream and downstream image measurement locations are centered at $x = 8.75\phi$ and $x = 33\phi$, respectively

Table 1 Measured properties of fluorescein and oxazine 725 in aqueous solutions (Soltys and Crimaldi 2011)

Dye	Peak Abs. (nm)	Peak Em. (nm)	ϵ (cm^{-1} M^{-1})
Fluorescein	491	514	1.40e5
Oxazine 725	656	668	2.33e5

3 Results

Instantaneous composite images of nondimensional scalar fields C_1 and C_2 for both the cylinder and no-cylinder configurations are shown for $s/\phi = 0.5$ and $Re_\phi = 2000$ in Fig. 3. Here and elsewhere in the results section, scalar concentrations are normalized by the corresponding source concentration C_0. The spatial coordinates x and z are measured relative to the midpoint between the two nozzles (Fig. 2), and are nondimensionalized by the cylinder diameter ϕ as $x^* = x/\phi$ and $z^* = z/\phi$. The triangular color maps shown in the figure uniquely display local concentrations of the individual scalars, as well as any combination of the two. The concentration of the lower plume, C_1, is shown in varying shades of red, while the upper jet, C_2, is shown in varying shades of blue. Ambient fluid is shown as white, and mixtures of C_1 and C_2 are displayed as varying shades of purple. All possible mixtures are contained in the triangular region of colormap.

For the no-cylinder case in the upstream location (Fig. 3a), the scalars are advected by the flow and transported roughly parallel to each other. Turbulent flow structures are not sufficiently large or energetic to quickly promote significant lateral stirring, and there is minimal coalescence between red and blue filaments. The result is minimal mixing or reaction between the two scalars. Further downstream (Fig. 3b), turbulent stirring has had more time to promote filament coalescence as it continues to stretch and fold the scalar fields, leading to an increase in the total mixing or reaction.

In the cylinder case, a wake forms downstream of the cylinder that consists of relatively large and energetic vortex structures that promote lateral stirring of the scalars, increasing their interfacial length, facilitated mixing and interactions between the two scalars even at the upstream location (Fig. 3c). At the downstream location (Fig. 3d), repeated stretching and folding events have significantly diluted the concentrations of the scalar filaments by promoting enhanced molecular diffusion, and significant mixing between the two scalars is evidenced by the various shades of purple (note the different concentration triangle scale).

Time-averaged distributions of non-dimensional concentrations C_1 and C_2 for the cylinder and no-cylinder cases for $s/\phi = 0.5$ and $Re_\phi = 2000$, at the upstream and downstream locations, are shown in Fig. 4. Each panel in Fig. 4 corresponds to the cases and locations shown in Fig. 3 for the instantaneous concentration fields. The mean plumes spread laterally as they advect in the streamwise direction, with a corresponding decrease in mean concentrations. The spreading leads to overlap between the blue and red plumes, as evidenced in the figure by shades of purple. In the cylinder case (bottom), the obstacle wakes downstream of the cylinder greatly enhance mean dispersion and mixing, producing an increase in mean overlap.

Transverse profiles of the time-averaged non-dimensional plume concentrations from Fig. 4 are shown in Fig. 5. Each profile point represents a bin of 75 pixels in z

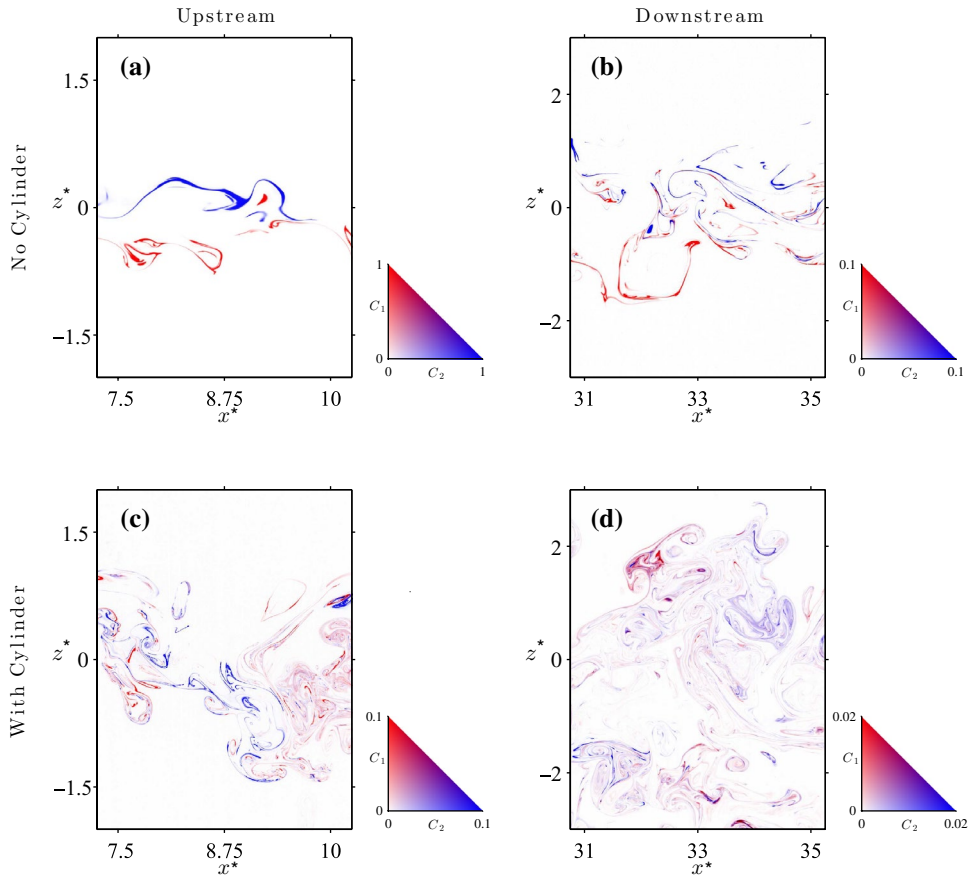

Fig. 3 Instantaneous distributions of non-dimensional concentrations C_1 and C_2 at the upstream and downstream locations for $s/\phi = 0.5$ and $Re_\phi = 2000$. The *top row* is for the no-cylinder case, and the *bottom row* is with the cylinder. A *color triangle* for C_1 (*shades of red*), C_2 (*shades of blue*), and various combinations of the two (*shades of purple*) is shown for each case

direction, averaged spatially in x across the central portion of the images from Fig. 4. For the no-cylinder cases (top), the mean concentration profiles are each symmetric with respect to the location of the respective nozzles; solid lines show Gaussian fits to these average concentration profiles. The no-cylinder concentration profiles also exhibit reflective symmetry about the flow centerline ($z = 0$). When the cylinder is introduced (bottom), the averaged plumes are no longer symmetric nor Gaussian due to the fact that each plume is exposed asymmetrically to the cylinder wake. Each mean plume exhibits a peak that is skewed towards the side of the respective nozzle location, since scalar from each nozzle passes preferentially to that side, and is preferentially entrained in the alternate vortices that are shed from that side of the cylinder. Due to the overall symmetry of the experiment, the two plumes still exhibit reflective symmetry about the centerline.

3.1 Effect of instantaneous flow process on total mixing and reaction

As discussed in Sect. 1.2, the mean local mixing parameter $\langle C_1, C_2\rangle$ is a metric for total reaction. As shown in Eq. 4, this reaction term can be decomposed as the sum of contributions from the mean, $\langle C_1\rangle\langle C_2\rangle$, and contributions from instantaneous processes, $\left\langle c_1' c_2' \right\rangle$. To investigate the relative contribution of these mean and instantaneous processes on the total reaction, separate cross section profiles of each term from Eq. 4 are shown in Fig. 6. Each term is calculated independently from 5000 instantaneous images for each of the experimental configurations and locations. For the non-cylinder case (Fig. 6a, b) dominant negative values of correlation (due to negative covariance) cause the product of the means to be initially larger than the total reaction. As turbulence brings filaments together and the mean plumes begin to overlap, the covariance becomes positive. At the downstream location, the covariance is positive across the entire profile. For the cylinder cases (Fig. 6c, d) all covariance terms are positive and contribute directly to the total reaction term.

The relative importance of instantaneous processes to the total reaction can be quantified via a normalized covariance given by

$$\beta = \left\langle c_1' c_2' \right\rangle / \langle C_1 C_2 \rangle , \tag{6}$$

which constitutes a ratio of the instantaneous reaction contributions compared to the total reaction. Profiles of β are plotted in Fig. 7 as a function of normalized transverse distance from the centerline z/w, where w is the local full width of the time-averaged reaction profile, $\langle C_1 C_2\rangle$. The width w is defined based on the location where $\langle C_1 C_2\rangle$

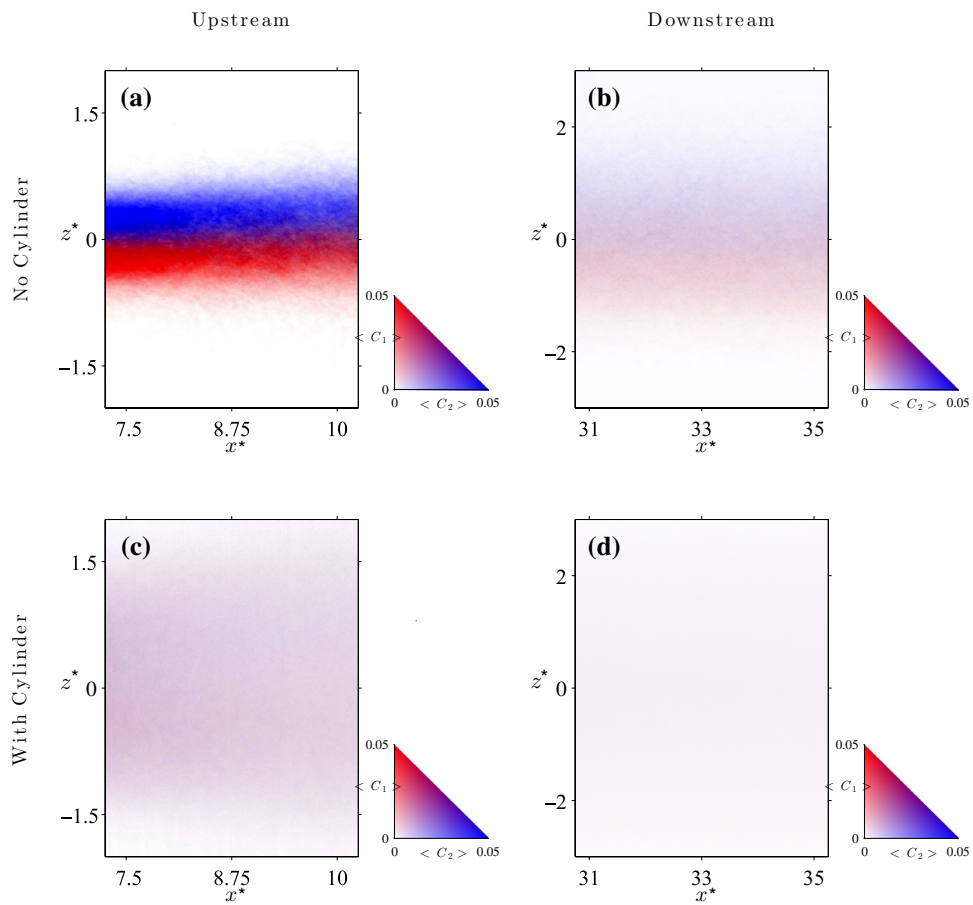

Fig. 4 Time-averaged distributions of non-dimensional concentrations C_1 and C_2 for $s/\phi = 0.5$ and $Re_\phi = 2000$, corresponding to the instantaneous distributions are shown in Fig. 1. The *top row* is for the no-cylinder case, and the *bottom row* is with the cylinder. The color scheme for $\langle C_1 \rangle$ (*shades of red*), $< C_2 >$ (*shades of blue*), and various combinations of the two (*shades of purple*) is shown for each case

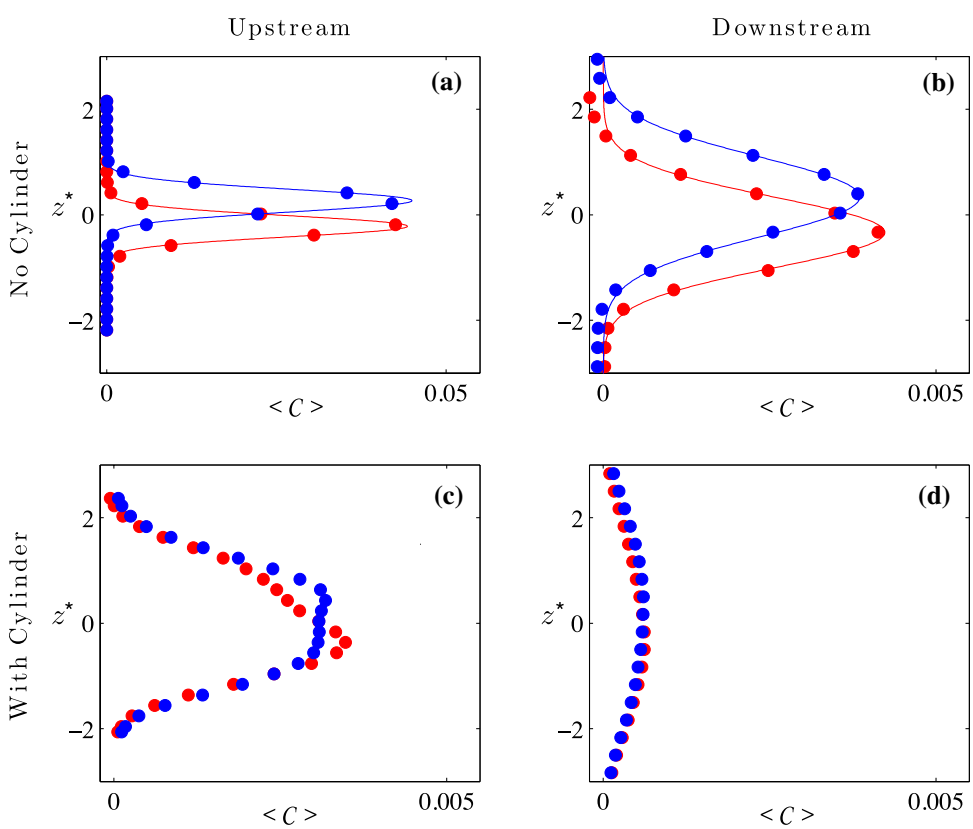

Fig. 5 Profiles of average non-dimensional concentrations $< C_1 >$ (*red*) and $< C_2 >$ (*blue*) for $s/\phi = 0.5$ and $Re_\phi = 2000$, corresponding to the four cases shown in Fig. 3. *Solid lines* in top figures are the Gaussian profiles fit to average concentration profiles. Note that the concentration scale is an order of magnitude lower for the *top right* and *bottom row* relative to the *top left row*

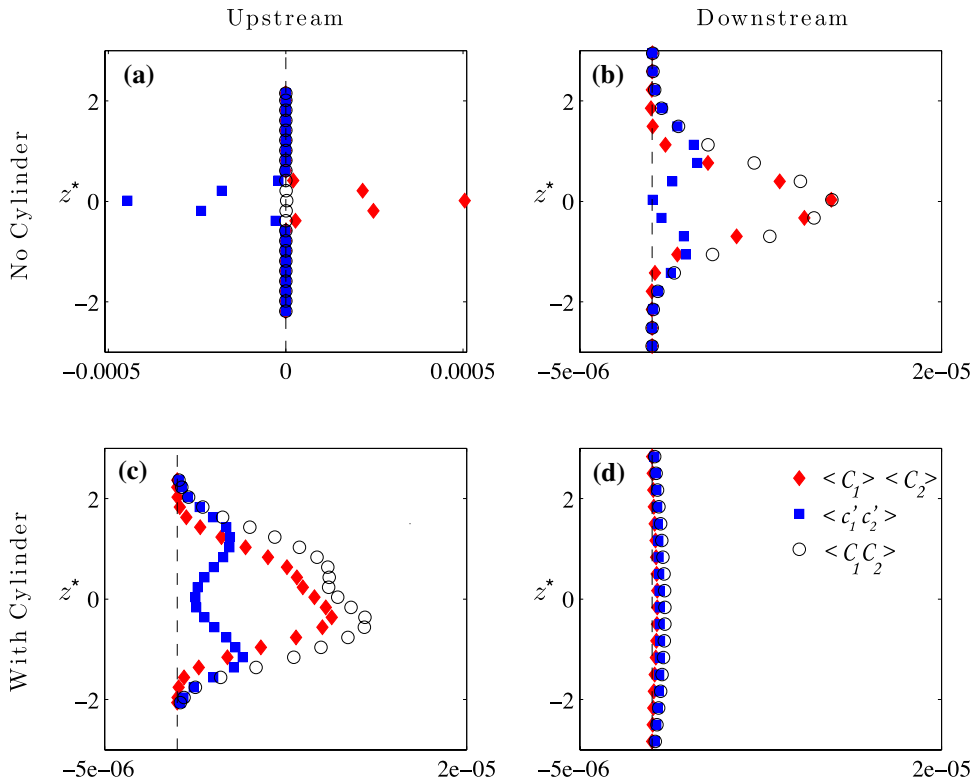

Fig. 6 Non-dimensional profiles of *red diamond* $< C_1 >< C_2 >$, *blue square* $< c_1' c_2' >$, and *open circle* $< C_1 C_2 >$ for $s/\phi = 0.5$ and $Re_\phi = 2000$, corresponding to the four cases shown in Fig. 3. Note that the scale is an order of magnitude lower for the *top right* and *bottom row* relative to the *top left row*

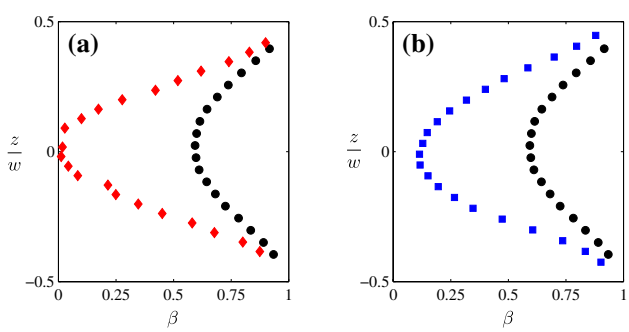

Fig. 7 Comparison of β for **a** *red diamond* no cylinder vs. *closed circle* cylinder at downstream location and **b** *blue square* upstream location vs. *closed circle* downstream location in cylinder case for $s/\phi = 0.5$ and $Re_\phi = 2000$

decays to 5% of the centerline maximum. Transverse profiles of β for the cylinder and no-cylinder cases are compared in Fig. 7a for the downstream location. For both cases, β increases monotonically with distance from the centerline, with $\beta \to 1$ for $z/w = \pm 0.5$. The presence of the cylinder produces a dramatic increase in β across the entire domain, with the most pronounced increase along the centerline, which rises to $\beta = 0.65$. Thus, for the downstream location, more than 65% of the scalar overlap is produced by contributions from the instantaneous physics. For both locations, nearly all of the overlap comes from the instantaneous processes near the edges $z/w = \pm 0.5$.

Transverse profiles of β at upstream and downstream locations are compared in Fig. 7b. The value of the ratio β increases with downstream distance due to rapid decay of $< C_1 >< C_2 >$. In the upstream location, values of β are relatively small $\beta \approx 0.1$ near the centerline, but grow rapidly away from the centerline. Taken together, Fig. 7a, b demonstrate that contributions to total reaction from instantaneous processes grow with streamwise distance from the source and with lateral distance from the centerline.

3.2 Effect of nozzle spacing and Reynolds number on total mixing and reaction

We now consider the effect of nozzle spacing s and Reynolds number Re_ϕ on mixing processes in the cylinder wake. The data presented so far correspond to $s/\phi = 0.5$ and $Re_\phi = 2000$. We now introduce two perturbations to this baseline case: in one case the nozzle spacing is reduced to $s/\phi = 0.25$, and in a second case the Reynolds number is increased to $Re_\phi = 5000$. Representative instantaneous concentration distributions at the downstream location for these two new cases are compared with that from the baseline case in Fig. 8. Figure 8a corresponds to the baseline case from Fig. 3d, with an instantaneous concentration distribution for the $s/\phi = 0.25$ case shown in Fig. 8b, and one from the $Re_\phi = 5000$ case shown in Fig. 8c. Corresponding profiles of the averaged non-dimensional total reaction

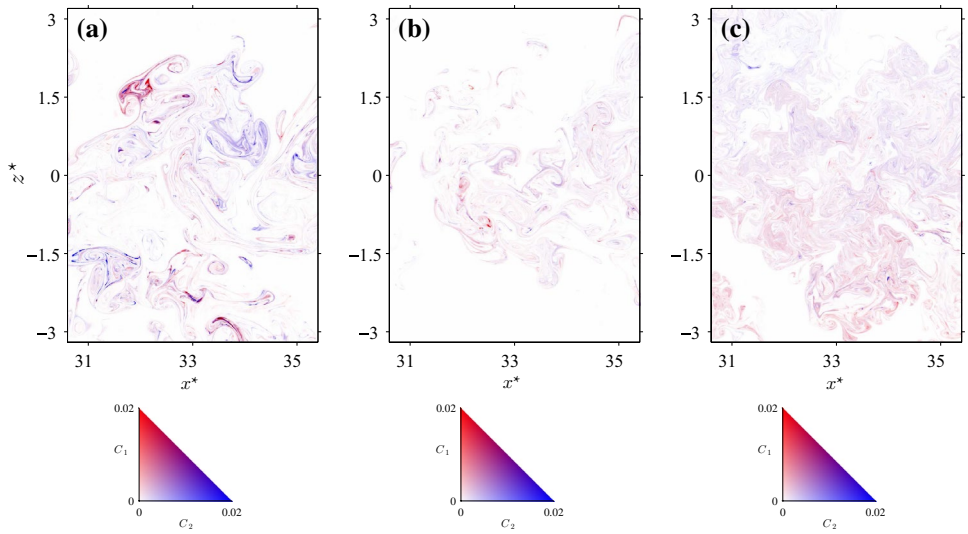

Fig. 8 Representative downstream distributions of instantaneous concentrations C_1 and C_2 for **a** $s/\phi = 0.5$ at $Re_\phi = 2000$, **b** $s/\phi = 0.25$ at $Re_\phi = 2000$, and **c** $s/\phi = 0.5$ at $Re_\phi = 5000$. The color scheme for C_1 (*shades of red*), C_2 (*shades of blue*), and various combinations of the two (*shades of purple*) is shown for each case

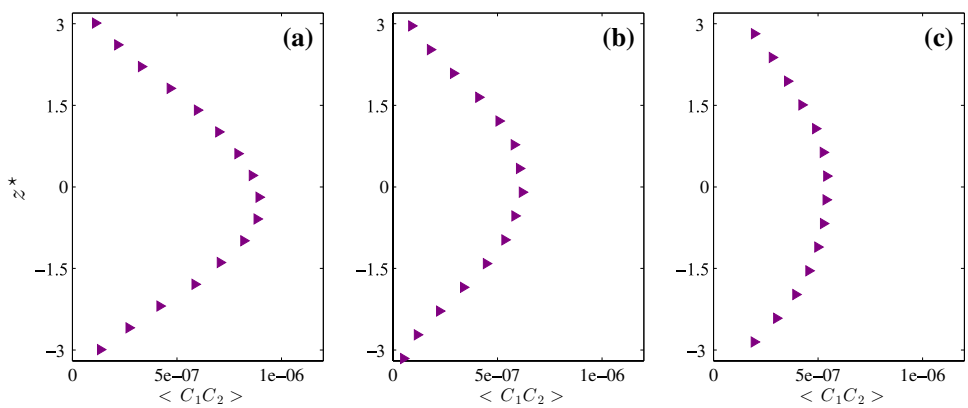

Fig. 9 Profiles of average scalar overlap $< C_1C_2 >$ corresponding to the three cases shown in Fig. 8. **a** $s/\phi = 0.5$ at $Re_\phi = 2000$, **b** $s/\phi = 0.25$ at $Re_\phi = 2000$, and **c** $s/\phi = 0.5$ at $Re_\phi = 5000$

product, $< C_1C_2 >$, are shown in Fig. 9. In the smaller nozzle spacing case (Fig. 9b), the centerline peak reaction rate is decreased and less mixing occurs in comparison with the baseline case. In the higher Reynolds number case (Fig. 9c), more mixing occurs across the flow (see Fig. 8c) but the total reaction product is reduced due to lower instantaneous concentrations associated with enhanced diffusion promoted by the extra stirring.

The effect of nozzle spacing and Reynolds number on transverse profiles of β at the downstream location is shown in Fig. 10. For the two nozzle spacings tested, the downstream profile of β is largely insensitive to the spacing (Fig. 10a). It appears that so long as the scalars are released close enough so that they are both mixed into the wake, the role of the instantaneous processes on mixing is unchanged with s. The effect of Reynolds number, however, is significant (Fig. 10b). In the more energetic flow regime, $< c_1'c_2' >$ continues to decay and β monotonically decreases, approaching a minimum value of 0.35 along the centerline. For both of the Reynolds number cases, the scalar covariance is the dominant term away from the centerline where

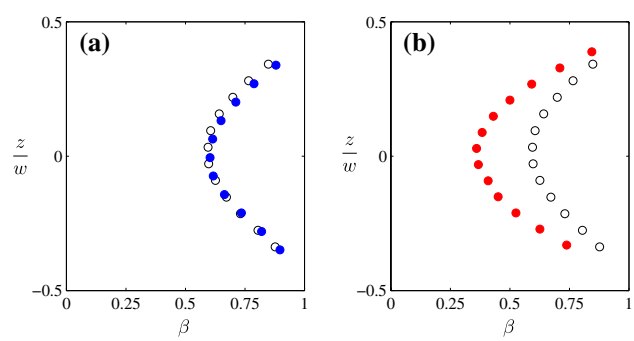

Fig. 10 Comparison of β for **a** *blue circle* $s/\phi = 0.25$ vs. *open circle* $s/\phi = 0.5$ at $Re_\phi = 2000$ and **b** *red circle* $Re_\phi = 5000$ vs. *open circle* $Re_\phi = 2000$ in $s/\phi = 0.5$. All experiments were taken at downstream location with the presence of cylinder

$\beta > 0.5$. In these regions, the product of the mean concentrations $< C_1 >< C_2 >$ is an extremely poor predictor of the mean scalar overlap $< C_1C_2 >$.

4 Conclusions

In this study, we use planar laser-induced fluorescence to investigate stirring and mixing of a pair of initially distant conservative scalars in the turbulent wake behind a cylindrical obstacle. The local scalar overlap C_1C_2 is used as a metric for second-order reaction rates between the two scalars in the low-*Da* limit; the scalar overlap quantifies the role of structured stirring on enhanced mixing and reaction between the initially distant scalars. We furthermore decompose the scalar overlap into two components that separately account for contributions from the mean and instantaneous scalar distributions. The results show presence of the obstacle wake generates significant mixing enhancement, with a significant portion of the reaction being associated with the instantaneous scalar covariance. The role of instantaneous processes grows strongly with distance downstream from the cylinder. As Reynolds number increases, the more energetic flow increases local dispersion and dilution of the scalar fields, resulting in a decrease in total reaction product. Although our studies were performed only in the low-*Da* limit, previous numerical investigations of simplified flows (Crimaldi et al. 2008) suggest that the reaction rate continues to be enhanced for finite *Da* grows, particularly for cases with energetic stirring.

A significant ecological implication of this study is that structured flow is a likely mechanism that facilitates successful coral reproduction. Coral heads and other benthic reef topology add structure to the ambient flow as water moves around the obstructions. In the reproduction strategy of broadcast spawning, male and female corals release egg and sperm from separate locations into the ambient water and rely primarily on the flow behavior to bring the gametes together to fertilize. This study suggests that the structured flow created due to the presence of a coral head can significantly increase the fertilization rate through enhanced contact between the initially distant egg and sperm.

Acknowledgements This work was supported by the National Science Foundation under Grants No. 0849695 and 1205816.

References

Adrian R, Christensen K, Liu ZC (2000) Analysis and interpretation of instantaneous turbulent velocity fields. Exp Fluids 29(3):275–290

Adrian RJ (2007) Hairpin vortex organization in wall turbulence a. Phys Fluids (1994-present) 19(4):041301

Batchelor G (1959) Small-scale variation of convected quantities like temperature in turbulent fluid part 1. General discussion and the case of small conductivity. J Fluid Mech 5(01):113–133

Breidenthal R (1981) Structure in turbulent mixing layers and wakes using a chemical reaction. J Fluid Mech 109:1–24

Cantwell BJ (1981) Organized motion in turbulent flow. Annu Rev Fluid Mech 13(1):457–515

Celik B, Beskok A (2009) Mixing induced by a transversely oscillating circular cylinder in a straight channel. Phys Fluids (1994-present) 21(7):073601

Crimaldi JP (2008) Planar laser induced fluorescence in aqueous flows. Exp Fluids 44(6):851–863. doi:10.1007/s00348-008-0496-2

Crimaldi JP, Browning HS (2004) A proposed mechanism for turbulent enhancement of broadcast spawning efficiency. J Mar Syst 49(1–4):3–18. doi:10.1016/j.jmarsys.2003.06.005

Crimaldi JP, Kawakami TR (2013) Reaction of initially distant scalars in a cylinder wake. Phys Fluids (1994-present) 25(5):053604

Crimaldi JP, Zimmer RK (2014) The physics of broadcast spawning in benthic invertebrates. Ann Rev Mar Sci 6:141–165

Crimaldi JP, Hartford JR, Weiss JB (2006) Reaction enhancement of point sources due to vortex stirring. Phys Rev E 74(1):016307

Crimaldi JP, Cadwell JR, Weiss JB (2008) Reaction enhancement of isolated scalars by vortex stirring. Phys Fluids 20(073):605

Deshmukh SR, Vlachos DG (2005) Novel micromixers driven by flow instabilities: application to post-reactors. AIChE J 51(12):3193–3204

Dong C, McWilliams JC (2007) A numerical study of island wakes in the Southern California Bight. Cont Shelf Res 27(9):1233–1248

Dong C, McWilliams JC, Shchepetkin AF (2007) Island wakes in deep water. J Phys Oceanogr 37(4):962–981

Ferrier G, Davies P, Anderson J (1996) Cover remote sensing observations of a vortex street downstream of an obstacle in an estuarine flow. Int J Remote Sens 17(1):1–8

Froncioni AM, Muzzio FJ, Peskin RL, Swanson PD (1997) Chaotic motion of fluid and solid particles in plane wakes. Chaos Solitons Fractals 8(1):109–130

Garrett C (1983) On the initial streakness of a dispersing tracer in two-and three-dimensional turbulence. Dyn Atmos Oceans 7(4):265–277

Guichard F, Bourget E (1998) Topographic heterogeneity, hydrodynamics, and benthic community structure: a scale-dependent cascade. Mar Ecol Prog Ser 171:59–70

Hasegawa D, Yamazaki H, Lueck RG, Seuront L (2004) How islands stir and fertilize the upper ocean. Geophys Res Lett 31(16). doi:10.1029/2004GL020143

Heywood KJ, Barton ED, Simpson JH (1990) The effects of flow disturbance by an oceanic island. J Mar Res 48(1):55–73

Hinch E (1999) Mixing: turbulence and chaos—an introduction. In: Mixing, Springer, pp 37–56

Jackson J (1986) Modes of dispersal of clonal benthic invertebrates: consequences for species' distributions and genetic structure of local populations. Bull Mar Sci 39(2):588–606

Jung C, Tél T, Ziemniak E (1993) Application of scattering chaos to particle transport in a hydrodynamical flow. Chaos Interdiscip J Nonlinear Sci 3(4):555–568

Károlyi G, Péntek Á, Toroczkai Z, Tél T, Grebogi C (1999) Chemical or biological activity in open chaotic flows. Phys Rev E 59(5):5468

Károlyi G, Péntek A, Scheuring I, Tél T, Toroczkai Z (2000) Chaotic flow: the physics of species coexistence. Proceedings of the National Academy of Sciences, vol 97, No. 25, pp 13661–13665

Kastrinakis E, Nychas S (1998) Mixing at high Schmidt numbers in the near wake of a circular cylinder. Chem Eng Sci 53(23):3977–3989

Mao KW, Toor HL (1971) Second-order chemical reactions with turbulent mixing. Ind Eng Chem Fundam 10(2):192–197. doi:10.1021/i160038a002

Mi J, Zhou Y, Nathan GJ (2004) The effect of reynolds number on the passive scalar field in the turbulent wake of a circular cylinder. Flow Turbul Combust 72(2–4):311–331

Miller K, Mundy C (2003) Rapid settlement in broadcast spawning corals: implications for larval dispersal. Coral Reefs 22(2):99–106

Pratt KR, Meiss JD, Crimaldi JP (2015) Reaction enhancement of initially distant scalars by Lagrangian coherent structures. Phys Fluids (1994-present) 27(3):035106

Richards K (1990) Physical processes in the benthic boundary layer. Philos Trans R Soc Lond Ser A Math Phys Sci 331(1616):3–13

Richards KJ, Brentnall SJ (2006) The impact of diffusion and stirring on the dynamics of interacting populations. J Theor Biol 238(2):340–347

Sandulescu M, López C, Hernández-García E, Feudel U (2008) Plankton blooms in vortices: the role of biological and hydrodynamic time scales. arXiv:08023973 (preprint)

Scheuring I, KÁrolyi G, PÉntek A, TÉl T, Toroczkai Z (2000) A model for resolving the plankton paradox: coexistence in open flows. Freshw Biol 45(2):123–132

Scheuring I, Károlyi G, Toroczkai Z, Tél T, Péntek A (2003) Competing populations in flows with chaotic mixing. Theor Popul Biol 63(2):77–90

Soltys MA, Crimaldi JP (2015) Joint probabilities and mixing of isolated scalars emitted from parallel jets. J Fluid Mech 769:130–153

Soltys MA, Crimaldi JP (2011) Scalar interactions between parallel jets measured using a two-channel PLIF technique. Exp Fluids. doi:10.1007/s00348-010-1019-5

Tel T, Károlyi G, Péntek A, Scheuring I, Toroczkai Z, Grebogi C, Kadtke J (2000) Chaotic advection, diffusion, and reactions in open flows. Chaos Interdiscip J Nonlinear Sci 10(1):89–98

Toroczkai Z, Károlyi G, Péntek Á, Tél T, Grebogi C (1998) Advection of active particles in open chaotic flows. Phys Rev Lett 80(3):500

Wang CT, Hu YC (2010) Mixing of liquids using obstacles in y-type microchannels. Tamkang J Sci Eng 13:385–394

Ziemniak EM, Jung C, Tél T (1994) Tracer dynamics in open hydrodynamical flows as chaotic scattering. Phys D Nonlinear Phenom 76(1):123–146